The Hidden Markov Model Reveals the Changes in Brain Dynamics Among Patients with End-Stage Renal Disease under Different Dialysis Methods

DANJIE SUN[1], WEIKAI LI[1,2], HUAN YU[3], XIAOFENG CHEN[1], and CHAOYANG ZHANG[4]
[1]School of Mathematics and Statistics, Chongqing Jiaotong University, Chongqing 404100, China
[2]School of Computer Science and Technology, Shandong Jianzhu University, Jinan 250101, China
[3]Department of Radiology, Liangxiang Hospital, Fangshan District, Beijing 102400, China
[4]Department of Nephrology, First Medical Center of Chinese PLA General Hospital, Beijing 100853, China

Corresponding author: Weikai Li (e-mail: leeweikai@outlook.com).

This work was partly supported by the National Natural Science Foundation of China (62306051,62481540175), the Scientific and the Technological Research Program of Chongqing Municipal Education Commission (KJQN202300718, KJZD-K202400703) and the Natural Science Foundation of Chongqing (CSTB2023NSCQ-LZX0092).

ABSTRACT Patients with end-stage renal disease often exhibit attention, memory, and executive dysfunction, reducing quality of life and increasing mortality risk. Hemodialysis and peritoneal dialysis are common treatments, but their effects on dynamic brain organization remain unclear. Resting-state functional magnetic resonance imaging data were collected from healthy controls and patients undergoing hemodialysis or peritoneal dialysis. Dynamic functional connectivity analysis with hidden Markov modeling and support vector machine classification characterized temporal and network alterations. Hemodialysis patients showed higher fractional occupancy ($p = 0.0015$, $d = 1.03$) and longer life time ($p = 0.0066$, $d = 0.87$) in State 1, indicating rigid network engagement. Peritoneal dialysis patients had preserved state proportions but elevated switching rates (PD vs NC: $p = 0.0222$, $d = 0.58$; PD vs HD: $p = 0.0022$, $d = 0.99$), reflecting excessive state transitions. Functional analysis revealed frontoparietal and dorsal attention network abnormalities in hemodialysis patients, whereas peritoneal dialysis patients displayed default mode network imbalances.Support vector machine classification confirmed these patterns (highest AUC = 0.876). Hemodialysis patients exhibited more rigid and less adaptive dynamics, while peritoneal dialysis patients showed hyperactive but unstable transitions. Dialysis-specific alterations underscore the impact of treatment type on neural dynamics and suggest that brain network metrics may serve as sensitive imaging biomarkers for early cognitive impairment in end-stage renal disease.

INDEX TERMS Cognitive impairment, Dialysis modality, Dynamic functional connectivity, Support vector machine

I. INTRODUCTION

CHRONIC kidney disease (CKD) is a progressive disease resulting from multiple etiological factors, including diabetes, hypertension, and glomerulonephritis [1], [2]. It is defined by a sustained reduction in glomerular filtration rate (GFR) [3]. As the disease progresses, a subset of patients develops end-stage renal disease (ESRD), necessitating renal replacement therapies such as hemodialysis (HD), peritoneal dialysis (PD), or kidney transplantation [4]. Epidemiological evidence indicates that cognitive impairment is prevalent among ESRD patients, with deficits commonly observed in attention, processing speed, executive function, and memory. The reported prevalence of cognitive impairment ranges from 25–51% in patientsnot yet on dialysis [5] , 30–70% in HD patients [6], [7], and 19–29% in PD patients [8], with increasing incidence associated with advancing age and disease duration. Cognitive decline not only diminishes quality of life and social functioning but also correlates with adverse clinical outcomes. However, conventional cognitive assessment tools, such as the Mini-Mental State Examination (MMSE) and the Montreal Cognitive Assessment (MoCA), demonstrate limited sensitivity in detecting mild cognitive impairments. Similarly, standard structural magnetic resonance imaging (MRI) often fails to detect subtle cerebral

alterations. In recent years, resting-state functional MRI (rs-fMRI) has emerged as a promising non-invasive technique [9] for investigating the neural mechanisms underlying cognitive impairment in ESRD, offering potential for the identification of early biomarkers and improved clinical management.

Most traditional studies of resting-state functional connectivity (FC) operate under the assumption that brain networks remain temporally invariant throughout the scanning period. This static analytical approach is insufficient to fully capture the dynamic and time-varying nature of brain activity [10]–[15]. Accumulating evidence suggests that functional connectivity exhibits temporal fluctuations and is closely associated with cognitive states, psychiatric disorders, and neurological conditions. Dynamic functional connectivity (dFC) enables the detection of recurrent transitions between brain networks, revealing temporal features that cannot be captured using static FC approaches. In the context of ESRD, particularly under different dialysis modalities, investigations into brain network dynamics remain limited, despite their potential significance in elucidating the mechanisms of cognitive dysfunction [16]–[19].

Current dFC methodologies, such as the sliding window approach and leading eigenvector dynamics analysis (LEiDA), have been widely employed in resting-state fMRI studies. The sliding window method estimates time-varying correlations by computing connectivity within a moving window; however, its outcomes are highly sensitive to the selection of window length, shape, and overlap, which lack universally optimal parameters. Moreover, this approach suffers from limited temporal resolution—short windows increase temporal sensitivity but may introduce instability, whereas long windows provide smoother estimates but obscure rapid state transitions. It also assumes local stationarity of neural signals, making it less suitable for capturing nonstationary dynamics and possibly introducing spurious fluctuations in connectivity. LEiDA, on the other hand, characterizes dynamic brain activity by tracking the leading eigenvector of instantaneous phase coherence, thereby revealing recurrent patterns of whole-brain synchronization. Despite its strengths in identifying global phase-alignment states, LEiDA remains sensitive to noise and parameter selection, and it primarily reflects dominant connectivity patterns while potentially overlooking subtler or transient dynamics. In addition, its computational complexity can be high when applied to large-scale data, which may limit its practicality in clinical populations. [20]–[27].

In contrast, the hidden Markov model (HMM) provides a more flexible and statistically principled framework for modeling dynamic brain states [28], [29]. HMM does not rely on predefined temporal windows or phase-dominant components; instead, it directly estimates the probability of latent brain state activation at each time point. This probabilistic representation allows precise characterization of state transitions and accommodates nonstationary neural signals without assuming temporal smoothness. Previous research has demonstrated that HMM can effectively identify dynamic differences between healthy individuals and patient populations [30]–[32]. Its related indicators, such as fractional occupancy (FO), life time (LT), and number of transitions (NT), provide valuable information for the stability and adaptability of brain networks. Based on this theoretical framework, we hypothesize that ESRD patients undergoing different dialysis modalities may exhibit distinct alterations in dynamic brain network patterns. These changes may contribute to a deeper understanding of cognitive impairment and provide potential neuroimaging biomarkers.

In the present study, we applied the HMM framework to resting-state fMRI data from ESRD patients. We conducted a systematic comparison of dynamic brain network characteristics among healthy controls (normal control, NC), HD patients, and PD patients. Furthermore, we integrated machine learning techniques with cognitive assessments to enhance the interpretability of our findings. We hypothesize that HD and PD patients exhibit distinct patterns of dynamic connectivity within key functional networks, and these features may serve as important foundations for understanding cognitive impairment and identifying potential neuroimaging biomarkers.

II. MATERIALS AND METHODS

A. DATA ACQUISITION

A total of 44 patients with ESRD and 47 healthy controls (normal control, NC) were recruited for this study. ESRD patients were further categorized into the peritoneal dialysis group (PD, n = 25) and the hemodialysis group (HD, n = 19) based on their respective treatment modalities. All participants were matched with the control group in terms of age, sex, and years of education.

The inclusion criteria for ESRD patients were as follows: (i) diagnosis of ESRD in accordance with the National Kidney Foundation Kidney Disease Outcomes Quality Initiative (NKF KDOQI) guidelines; (ii) undergoing maintenance dialysis two to three times per week for a minimum of three months; (iii) no prior history of kidney transplantation or acute renal failure.

The exclusion criteria for ESRD patients were as follows: (i) history of alcohol or substance abuse; (ii) history of traumatic brain injury or psychiatric disorders; (iii) presence of other neurological conditions such as stroke or brain tumors.

For healthy volunteers, the inclusion criteria were defined as: (i) matching with ESRD patients in age, sex, and educational background; (ii) normal renal function confirmed by clinical evaluation. The exclusion criteria for healthy controls were identical to those applied to the ESRD group.

B. DATA PROCESSING AND ANALYSIS

Demographic information including age, sex, and education was collected. MRI data were acquired on a Magnetom Skyra 3.0 T scanner (Siemens, Germany) using a 32-channel

phased-array head coil. Both structural and functional images were obtained.

For structural imaging, a 3D T1-weighted MP-RAGE sequence was used with the following parameters: repetition time (TR) = 2000 ms, inversion time (TI) = 880 ms, echo time (TE) = 2.01 ms, flip angle (FA) = 8°, matrix = 256 × 256, field of view (FOV) = 256 × 256 mm^2, sagittal total thickness = 208 mm, thickness = 1 mm.

For functional imaging, single excitation gradient echo-echo planar imaging (SS-GRE-EPI) was applied with the following parameters: TR = 2000 ms, TE = 30 ms, FA = 90°, matrix = 64 × 64, FOV = 224 × 224 mm^2, layer thickness = 4 mm, number of layers = 36, number of repetitions = 180, fat suppression on, and parallel imaging factor = 2. During the scan, participants were instructed to close their eyes, remain still, stay awake, and stay relaxed.

Preprocessing was performed using SPM8 (http://www.fil.ion.ucl.ac.uk/spm) and DPARSFA toolboxes [33]. The first 10 time points of each scan were removed to avoid signal instability. The remaining images were normalized to MNI space and resampled to 3 × 3 × 3 mm^3 voxels. Confounding covariates including cerebrospinal fluid, white matter signals, and head motion were regressed out using the Friston model. A band-pass filter of 0.01–0.08 Hz was applied and linear trends were removed. The preprocessed fMRI data were parcellated into 90 regions of interest (ROIs) based on the Automated Anatomical Labeling (AAL90) atlas [34].

C. COGNITIVE ASSESSMENT

Cognitive function was assessed with the Mini-Mental State Examination (MMSE) and the Montreal Cognitive Assessment (MoCA) [35]. The MMSE has been widely used to screen for moderate to severe cognitive impairment and is particularly suitable for individuals with lower educational levels. MoCA complements MMSE and is more sensitive for detecting mild cognitive impairment. All participants completed MMSE and MoCA assessments within one week prior to MRI scanning to quantify overall cognitive function.

D. HIDDEN MARKOV MODELING

Dynamic brain states were analyzed using the hidden Markov model (HMM). The assumption of HMM in brain dynamics is that fluctuations of brain activity can be explained by a finite number of discrete and recurring hidden states through the time series of brain regions of interest (ROIs). At each time point t, the brain is assumed to be in a latent state Z_t. The distribution of each hidden state j was modeled by a multivariate Gaussian distribution, parameterized by a mean activation vector $\boldsymbol{\mu}_j$ and covariance matrix $\boldsymbol{\Sigma}_j$, as shown in Eq. (1):

$$X_t \mid Z_t = j \sim \mathcal{N}(\boldsymbol{\mu}_j, \boldsymbol{\Sigma}_j), \tag{1}$$

where $\boldsymbol{\mu}_j$ represents the average functional activity of state j, and $\boldsymbol{\Sigma}_j$ (a 90×90 covariance matrix) reflects the functional connectivity structure among brain regions within that state.

Another essential property of HMM is the probability of transitions between states, which can be described by a transition probability matrix A_{ij}. It defines the likelihood of switching from state i at time $t-1$ to state j at time t. This is expressed in Eq. (2):

$$\Pr(Z_t = j) = \sum_{i=1}^{M} A_{ij} \Pr(Z_{t-1} = i), \tag{2}$$

where M is the total number of hidden states. The most probable state at time t is selected according to the maximum posterior probability.

The HMM was implemented using the Hidden Markov Model–Multivariate Autoregressive (HMM-MAR) toolbox (https://github.com/OHBA-analysis/HMM-MAR) in MATLAB [36], with inference performed using variational Bayesian methods. For each participant, time series from 90 ROIs (170 time points) were extracted, normalized, and concatenated across subjects as model input.

To determine the optimal number of hidden states, we followed previous studies and systematically varied M from 2 to 20. For each M, the model was trained 100 times with different random initializations to ensure convergence stability [37]. Model performance was evaluated using two complementary criteria: variational free energy and state fractional occupancy. Variational free energy quantifies the trade-off between model fit and complexity—lower values indicate a more optimal balance and better convergence. State fractional occupancy reflects the proportion of time each state is active across the time series, ensuring that all states are meaningfully utilized rather than being redundant or underrepresented.

By averaging the free energy and median fractional occupancy across repetitions, we identified $M = 4$ as the optimal number of states. This choice satisfied two criteria: (1) the model achieved the lowest average free energy, and (2) all states exhibited stable and non-negligible occupancy, indicating effective utilization. This selection balances model parsimony and representational capacity, avoids overfitting, and ensures robust characterization of dynamic brain states.

Each identified state was subsequently represented by its Gaussian parameters ($\boldsymbol{\mu}_j, \boldsymbol{\Sigma}_j$), allowing detailed examination of the corresponding dynamic functional connectivity patterns.

To better explain the changes in the connection patterns of brain networks, we divided the 90 ROIs into 7 brain networks defined by Yeo et al. [38] (Default Mode Network, DMN; Frontoparietal Network, FPN; Salience Network, SN; Dorsal Attention Network, DAN; Sensorimotor Network, SMN; Visual Network, VN; Limbic Network, LN). This allowed us to further analyze the connection patterns within and between networks in each state.

E. TEMPORAL FEATURES AND STATISTICAL ANALYSIS

To quantify group differences (NC, HD, PD) in the dynamic properties of hidden brain states, three temporal met-

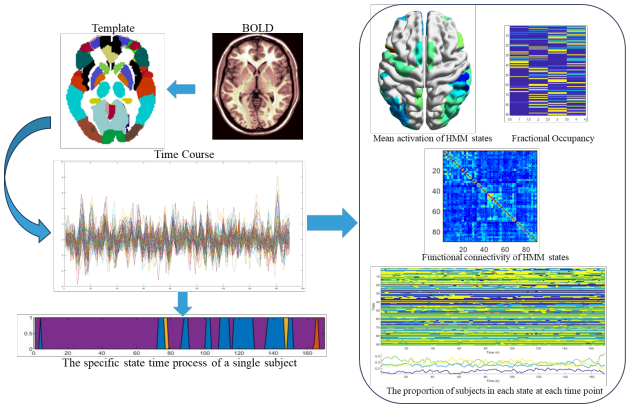

FIGURE 1: Schematic illustration of the hidden Markov model (HMM) analysis pipeline. For each subject, BOLD signals were first parcellated according to the AAL atlas to extract regional time series. These time series were then modeled using HMM to infer dynamic brain states, yielding individual state transition sequences across 170 time points. From the estimated states, several features were derived, including the mean activation of HMM states, fractional occupancy, state-specific functional connectivity patterns, and the proportion of subjects occupying each state at each time point.

rics were computed from the decoded state time series, for each participant. 1. Fractional occupancy (FO): the proportion of time spent in a specific state relative to total scan duration, reflecting overall tendency and persistence in that state. 2. Life Time (LT): the average duration of consecutive time points in a given state, reflecting stability and continuity of that state. 3. Switching rate (SWT): the total number of transitions between states divided by scan length, reflecting the frequency and flexibility of state switching.

Group differences in FO, LT, and SWT were assessed using two-sample t-tests for each pair of groups. Effect sizes were quantified using Cohen's d to provide standardized measures of group differences beyond statistical significance. All statistical analyses were conducted in MATLAB, and significance was set at $p < 0.05$.

F. SUPPORT VECTOR MACHINE CLASSIFICATION

Support vector machine (SVM) classification was applied to differentiate between groups. Input features included fractional occupancy (FO), mean lifetime (LT), switching rate (SWT), and static functional connectivity (sFC). For the sFC features, a one-way analysis of variance (ANOVA) was conducted across the three groups (NC, HD, PD), and only edges with significant group differences ($p < 0.001$) were retained:

$$F = \frac{\mathrm{MS}_{\text{between}}}{\mathrm{MS}_{\text{within}}}, \quad p = P(F \geq F_{\text{obs}}), \tag{3}$$

where $\mathrm{MS}_{\text{between}}$ and $\mathrm{MS}_{\text{within}}$ are the mean square values between and within groups, respectively.

All features were rescaled to the range $[-1, 1]$:

$$x_i^{\text{norm}} = \frac{2(x_i - \min(x))}{\max(x) - \min(x)} - 1. \tag{4}$$

The binary SVM classifier aimed to find the optimal separating hyperplane

$$f(\mathbf{x}) = \mathbf{w}^T \phi(\mathbf{x}) + b, \tag{5}$$

by solving the optimization problem

$$\begin{aligned} \min_{\mathbf{w},b,\boldsymbol{\xi}} \quad & \frac{1}{2}\|\mathbf{w}\|^2 + C\sum_{i=1}^{N} \xi_i, \\ \text{s.t.} \quad & y_i \left(\mathbf{w}^T \phi(\mathbf{x}_i) + b\right) \geq 1 - \xi_i, \\ & \xi_i \geq 0, \end{aligned} \tag{6}$$

where $y_i \in \{0, 1\}$ denotes the class label, C is the penalty parameter, and $\phi(\cdot)$ represents the feature mapping induced by the kernel. A radial basis function (RBF) kernel was used:

$$\kappa(\mathbf{x}_i, \mathbf{x}_j) = \exp(-\gamma \|\mathbf{x}_i - \mathbf{x}_j\|^2), \tag{7}$$

with γ controlling the kernel width. The decision function is given by

$$\hat{y} = \text{sign}\left(\sum_{i=1}^{N} \alpha_i y_i \kappa(\mathbf{x}_i, \mathbf{x}) + b\right), \tag{8}$$

where α_i are Lagrange multipliers.

Model parameters C and γ were optimized by grid search with leave-one-out cross-validation (LOOCV). Classification tasks included three pairwise comparisons (NC vs. HD, NC vs. PD, HD vs. PD) and one three-class classification (NC, HD, PD) using the one-vs-one scheme with majority voting.

Model performance was quantified using accuracy, F1 score, receiver operating characteristic (ROC) curves, and the area under the curve (AUC).

Accuracy is defined as the proportion of correctly classified samples:

$$\text{Accuracy} = \frac{TP + TN}{TP + FP + TN + FN}, \tag{9}$$

where TP, TN, FP, and FN represent true positives, true negatives, false positives, and false negatives, respectively.

The F1 score is defined as the harmonic mean of precision and recall:

$$\text{F1} = \frac{2 \cdot \text{Precision} \cdot \text{Recall}}{\text{Precision} + \text{Recall}}, \tag{10}$$

with

$$\text{Precision} = \frac{TP}{TP + FP}, \quad \text{Recall} = \frac{TP}{TP + FN}. \tag{11}$$

For multi-class classification, the one-vs-one strategy was applied, and the macro-averaged F1 score was used:

$$\text{F1}_{\text{macro}} = \frac{1}{K}\sum_{k=1}^{K} \text{F1}_k, \tag{12}$$

where K denotes the number of classes and F1_k is the F1 score for class k.

ROC curves are obtained by plotting the true positive rate (TPR) against the false positive rate (FPR):

$$\text{TPR} = \frac{TP}{TP + FN}, \quad \text{FPR} = \frac{FP}{FP + TN}. \tag{13}$$

The area under the ROC curve (AUC) is calculated as:

$$\text{AUC} = \int_0^1 \text{TPR}(\text{FPR})\, d(\text{FPR}), \tag{14}$$

which reflects the overall discriminative ability of the classifier, independent of threshold selection.

G. IDENTIFICATION OF CONSENSUS CONNECTIONS

To determine the impact of different dialysis modalities on functional connectivity in ESRD patients, we compared the mean connectivity strength of each edge between the HD and PD groups. Two-sample t-tests were applied to identify significant differences, and only those edges that consistently survived across iterations were retained as consensus connections. This strategy reduced false positives caused by random fluctuations and highlighted highly stable abnormalities. Finally, the identified consensus connections were mapped from the AAL90 template to the Yeo7 functional networks, allowing us to investigate the influence of dialysis modalities on brain network organization at the systems level.

H. CORRELATION WITH COGNITIVE FUNCTION

To explore the clinical relevance of dynamic features, correlations between dFC metrics and cognitive performance were examined. Spearman rank correlations were performed between FO, LT, and SWT and neuropsychological scores including MMSE and MoCA.

III. RESULTS

A. STATE CHARACTERISTICS

The HMM analysis identified four functional connectivity states that differed mainly in the dominant roles of specific networks. Each HMM state is described by the average activity intensity of 90 brain regions in Fig. 2 and the connection strength in Fig. 3 between the involved brain regions.

State 1 was characterized by strong connections within the FPN and VN, accompanied by increased activity in the SMN and DMN. Cross-network connections were relatively weaker, especially between subcortical structures and the FPN, DMN, and SN.

State 2 showed a prominent synergy between the VN and DMN, with strong connections concentrated within the visual cortex and the DMN. Weak connections were mainly observed between subcortical structures and the FPN and SMN.

State 3 was characterized by enhanced coupling between the FPN and subcortical structures, together with strong connections in the VN and SN. The SMN was relatively suppressed in this state.

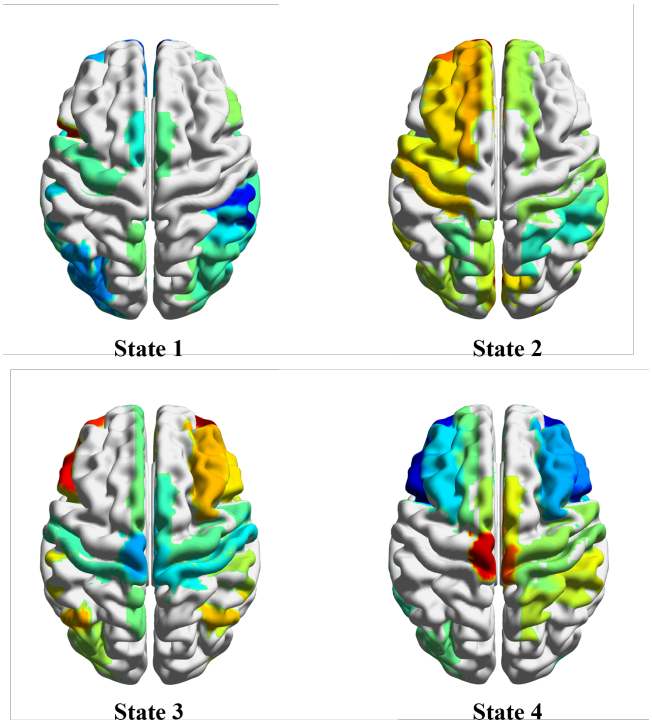

FIGURE 2: The activity intensity of brain regions in states 1-4.The 3D graphics in this figure were created using BrainNet Viewer Version 1.7 (https://www.nitrc.org/projects/bnv/).

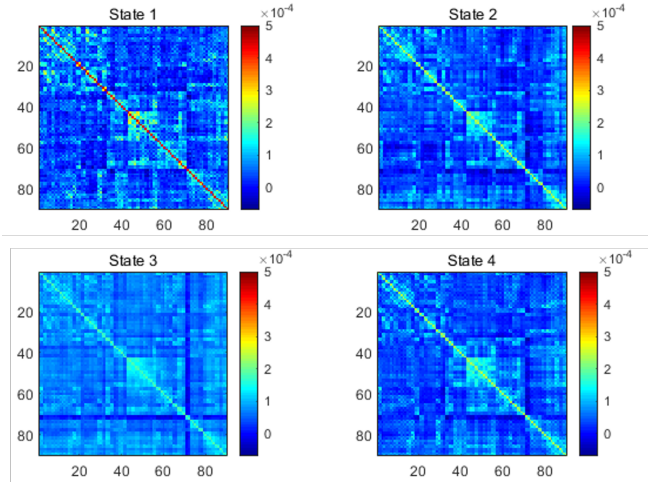

FIGURE 3: The functional connection mode of the latent state.

State 4 was marked by increased activity in the SMN and SN, while the VN and DMN maintained strong within-network connectivity. Overall, the four states reflected distinct organizational patterns of large-scale networks.

B. TEMPORAL PROPERTIES

We next compared the three groups with respect to FO, LT, and SWT. The detailed ANOVA and post-hoc results for all

temporal metrics are summarized in **TABLE 1**.

For FO, significant group differences were observed in State 1 ($p < 0.001$) and State 3 ($p = 0.048$). In State 1, HD patients showed markedly higher FO compared with both PD ($p = 0.0015$, $d = -1.03$) and NC ($p < 0.001$, $d = 1.35$), indicating that hemodialysis patients were more likely to remain in this state. In contrast, FO in State 3 was significantly lower in HD patients than in NC ($p = 0.016$, $d = -0.67$) and showed a marginally lower trend compared with PD ($p = 0.0619$). No significant group differences were found in States 2 or 4.

For LT, ESRD patients exhibited significantly longer LT in State 1 compared with NC ($p = 0.002$, $d = 0.67$), suggesting that they tended to stay longer in this state. Further three-group comparisons revealed that HD patients had significantly higher LT in State 1 ($p < 0.001$), with post-hoc tests showing higher values in HD than in both PD ($p = 0.0066$, $d = -0.87$) and NC ($p < 0.001$, $d = 1.22$). No other states showed significant group differences.

For SWT, significant differences were found across groups ($p < 0.01$). PD patients exhibited significantly higher switching rates than both NC ($p = 0.0222$, $d = 0.58$) and HD ($p = 0.0022$, $d = 0.99$), indicating greater temporal variability in brain state transitions. No significant difference was observed between HD and NC.

Overall, HD patients tended to remain longer in a specific state (State 1), whereas PD patients exhibited higher transition frequencies, reflecting distinct patterns of dynamic brain network flexibility between dialysis modalities.

C. SVM CLASSIFICATION

In the SVM classification analysis, we first applied one-way ANOVA based on static functional connectivity to identify 233 functional connections with significant group differences, thereby reducing the feature space while preserving the most discriminative connections. These features were then concatenated with the FO, LT, and SWT indices derived from each state to construct the final feature set for classification.

In pairwise classification, the best performance was achieved in distinguishing NC from HD, with an accuracy of 91% and an AUC of 0.876. The accuracy for NC versus PD was 83% (AUC = 0.855), while that for HD versus PD was 84% (AUC = 0.834), indicating that the two dialysis modalities also exhibited considerable discriminability.

In the three-class classification task, the model achieved an overall accuracy of 80% with a macro-F1 score of 0.78, suggesting balanced performance across the three groups. ROC curve analysis further revealed that NC was recognized most accurately (AUC = 0.882), followed by HD (AUC = 0.869), whereas PD was more challenging to classify (AUC = 0.845) and tended to be misclassified as NC or HD.The overall micro-average AUC reached 0.873. These results are illustrated in Fig. 4, which shows the ROC curves for the three-class classification task, further demonstrating that PD patients exhibit altered brain networks, but these alterations

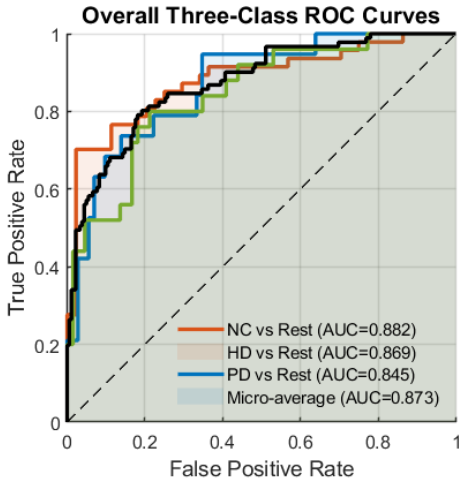

FIGURE 4: Receiver operating characteristic (ROC) curves for the overall three-class classification. One-vs-rest ROC curves are presented for each group (NC, HD, and PD), together with the micro-average curve across all classes. The corresponding area under the curve (AUC) values are reported in the legend.

are less pronounced than those in HD patients, reflecting an intermediate pattern of disruption.

D. CONSENSUS CONNECTIONS

In the comparison between PD and NC, a total of 95 consensus connections were identified. These abnormal connections were primarily distributed across the VN, the SN, the DMN, and subcortical regions. Enhanced coupling between the medial superior frontal gyrus and the anterior cingulate cortex indicated a compensatory upregulation within the DMN, whereas weakened connections between visual cortices such as the cuneus and middle occipital gyrus with the supramarginal gyrus suggested impaired pathways for visual information integration and attentional shifting. Moreover, several weakened connections between the supramarginal gyrus and the thalamus revealed reduced coordination between subcortical regions and the , which may compromise the selective modulation of sensory inputs.

In the comparison between HD and NC, 199 consensus connections were detected, reflecting more extensive and stronger abnormalities. These alterations involved the SN, SMN, VN, and subcortical regions. The most significant connections were largely characterized by strengthened intra-network coupling or bilateral homotopic synchronization, including enhanced connections between bilateral amygdala, hippocampus, occipital cortices, and supramarginal gyri. Such patterns suggest that the alterations in HD patients extend beyond inter-network interactions and involve pathological hyper-synchronization within networks. Particularly, the markedly increased coupling between bilateral auditory cortices and supramarginal gyrus within the SMN indicates abnormal processing or integration of external stimuli and

TABLE 1: Group comparisons of temporal properties (Fractional Occupancy, Mean Life Time, and Switching Rate) among PD, HD, and NC groups. Values represent ANOVA and post-hoc results. Significant results ($p < 0.05$) are shown in bold.

Metric	State	ANOVA p	PD–HD p	Cohen's d	PD–NC p	Cohen's d	HD–NC p	Cohen's d
FO	State 1	**0.0000**	**0.0015**	-1.0308	0.3465	0.2346	**0.0000**	1.3549
	State 2	0.2120	0.8879	-0.0432	0.1286	-0.3807	0.2313	-0.3285
	State 3	**0.0482**	0.0619	0.5838	0.5533	-0.1475	**0.0162**	-0.6715
	State 4	0.1312	0.1075	0.5006	0.0609	0.4716	0.8753	-0.0428
LT	State 1	**0.0000**	**0.0066**	-0.8700	0.1772	0.3374	**0.0000**	1.2188
	State 2	0.0898	0.2185	-0.3802	**0.0403**	-0.5171	0.3200	-0.2725
	State 3	0.1893	0.4002	0.2587	0.2622	-0.2798	0.1310	-0.4159
	State 4	0.6057	0.8799	-0.0463	0.3453	0.2352	0.4163	0.2224
SWT	–	**0.0046**	**0.0022**	0.9913	**0.0222**	0.5790	0.1329	-0.4138

FO = Fractional Occupancy; LT = Mean Life Time; SWT= Switching Rate; PD = Peritoneal Dialysis; HD = Hemodialysis; NC = Normal Control. Bold indicates $p < 0.05$. Post-hoc pairwise comparisons (PD–HD, PD–NC, HD–NC) were performed using two-sample independent t-tests, and Cohen's d values indicate effect sizes.

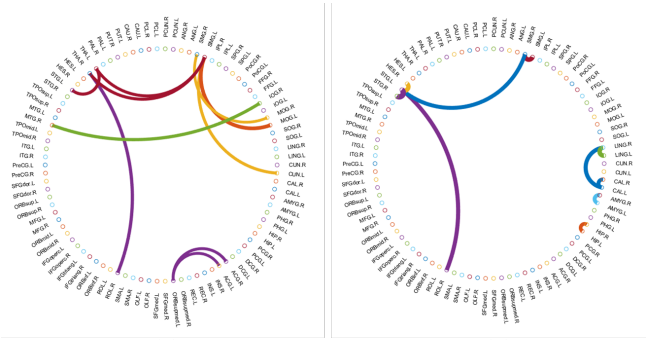

(a) (b)

FIGURE 5: The top 10 most significant consensus function connections identified in the comparisons of (a) PD versus NC and (b) HD versus NC.

motor planning, while the over-connectivity between the hippocampus and amygdala may reflect dysfunctional activity in emotion and memory circuits. The top 10 most significant consensus connections in PD patients and HD patients are respectively presented in Fig. III-D.

Taken together, PD patients exhibited relatively localized disruptions characterized by abnormal interactions between specific networks, whereas HD patients showed widespread abnormalities involving cortico-subcortical connectivity and large-scale disruptions in sensory and cognitive networks. This difference may be attributed to the distinct hemodynamic and metabolic effects of the two dialysis modalities, further revealing divergent mechanisms of brain functional alterations in ESRD.

E. COGNITIVE CORRELATION ANALYSIS

In addition, we examined the correlations between the dFC metrics and the cognitive scores.

In the NC group, none of the FO, LT, or SWT indices were significantly correlated with MMSE or MoCA ($|r| < 0.2$, $|p| > 0.2$). In the HD group, SWT showed a significant negative correlation with MoCA ($|r|$ = -0.596, $|p|$ = 0.007). In the PD group, LT in State 2 showed a moderate positive trend with MMSE ($|r|$ = 0.393, $|p|$ = 0.052).

In general, dFC metrics were more strongly related to cognitive decline in HD, while LT characteristics were more relevant in PD.

IV. DISCUSSION

This study compared ESRD patients undergoing different dialysis modalities to healthy controls using dynamic functional connectivity (DFC) analysis combined with SVM-based classification. The results revealed significant differences in both the temporal properties and topological organization of brain networks among groups.

In the temporal properties, HD patients exhibited markedly higher fractional occupancy and longer life time in State 1, indicating a prolonged persistence in a single, rigid brain network configuration. Such reduced flexibility suggests a decreased ability of large-scale neural systems to dynamically reconfigure in response to internal or external demands. From a neurobiological perspective, the intermittent hemodynamic instability, osmotic fluctuations, and recurrent toxin accumulation associated with hemodialysis may disrupt neuronal communication efficiency and impair the adaptability of functional networks, thereby contributing to the cognitive slowing and executive dysfunction frequently observed in HD patients.

In contrast, PD patients demonstrated state proportions and dwell times more comparable to those of healthy controls, reflecting relatively preserved network stability. However, their significantly higher switching rate suggested excessive transitions between brain states—a possible manifestation of compensatory hyper-flexibility. This pattern may represent an intermediate stage of neural reorganization, in which compensatory mechanisms attempt to preserve cognitive performance despite subtle structural or metabolic alterations. Clinically, this could correspond to mild cognitive inefficiency or attentional fluctuation in PD patients.

When further examined in the context of functional states, HD patients showed pronounced abnormalities in states dominated by the FPN and DAN, potentially explaining impairments in executive control and attentional regulation. In contrast, PD patients displayed a greater imbalance between the DMN and other large-scale systems, which may underlie

deficits in memory consolidation and self-referential processing. These modality-specific network alterations highlight that HD may exert a stronger disruptive effect on higher-order cognitive systems, whereas PD may induce subtler and partially compensatory reconfigurations.

The smaller number of abnormal connections in PD patients, primarily between the VN, SN, and DMN, indicates a reduced but not completely lost capacity for cross-network integration. For example, weakened coupling between visual regions and the supramarginal gyrus may hinder attentional reallocation, while altered SN–thalamic interactions could impair sensory filtering and salience detection. Conversely, HD patients exhibited nearly twice as many abnormal connections, with extensive intra-network hyper-synchronization and subcortical overconnectivity. Such pathological synchronization may reflect dedifferentiation a loss of functional specificity and could contribute to the broad cognitive and emotional disturbances often observed in these patients.

Taken together, these findings suggest that HD patients exhibit more rigid and less adaptive brain dynamics, whereas PD patients display hyperactive but unstable transitions, representing two distinct patterns of disrupted network flexibility in ESRD. The modality-specific alterations observed here provide insight into potential neural mechanisms linking dialysis-related physiological stress to cognitive dysfunction. These results suggest that brain network dynamics may serve as a sensitive neuroimaging biomarker for early cognitive impairment in ESRD.

Although our sample size was modest and cognitive assessments were limited to screening scales, which may have influenced the results, the findings remain informative. Future longitudinal and multimodal studies with larger cohorts are needed to confirm these observations.

V. LIMITATIONS

This study has several limitations. First, the sample size was relatively small, especially in the subgroups of ESRD patients under different dialysis modalities, which may reduce statistical power and the robustness of the findings. Future work should validate these results in larger and multicenter cohorts. Second, this was a cross-sectional study that only revealed differences in brain function between dialysis modalities, but it cannot determine causal relationships or long-term trajectories. Longitudinal follow-up studies are needed to address this issue. Third, the analysis was based solely on resting-state fMRI, without integration of structural imaging or metabolic measures, which limits the interpretation of ESRD-specific mechanisms such as uremic toxin accumulation and recurrent hemodynamic fluctuations. Fourth, cognitive assessment was restricted to scales such as MMSE and MoCA, which may not comprehensively capture multidimensional impairments in attention, executive function, and memory. More systematic neuropsychological testing should be considered in future work. Finally, although the machine learning models demonstrated good classification performance, external validation with larger samples and independent datasets is required to improve their clinical applicability.

VI. CONCLUSION

Patients with end-stage renal disease demonstrate distinct dynamic patterns of brain network activity that differ according to the type of dialysis treatment. Hemodialysis patients are predominantly characterized by increased cerebral network rigidity, whereas peritoneal dialysis patients exhibit a higher frequency of state transitions. These variations may be attributed to the differing hemodynamic and metabolic impacts associated with each dialysis modality. These findings indicate that changes in brain network dynamics could potentially serve as early neuroimaging biomarkers for cognitive decline in patients with end-stage renal disease undergoing different forms of dialysis.

ETHIC APPROVAL

Subjects signed an informed consent form and study was approved by the Ethics Committee of Liangxiang Teaching Hospital of Capital Medical University (no. 2016174).

REFERENCES

[1] A. S. Levey and J. Coresh, "Chronic kidney disease," The lancet, vol. 379, no. 9811, pp. 165–180, 2012.
[2] R. Noble and M. W. Taal, "Epidemiology and causes of chronic kidney disease," Medicine, vol. 47, no. 9, pp. 562–566, 2019.
[3] G. J. Schwartz and S. L. Furth, "Glomerular filtration rate measurement and estimation in chronic kidney disease," Pediatric nephrology, vol. 22, no. 11, pp. 1839–1848, 2007.
[4] G. M. Fleming, "Renal replacement therapy review: past, present and future," Organogenesis, vol. 7, no. 1, pp. 2–12, 2011.
[5] C. M. Burns, D. S. Knopman, D. E. Tupper, C. S. Davey, Y. M. Slinin, K. Lakshminarayan, R. C. Rossom, S. L. Pederson, D. T. Gilbertson, and A. M. Murray, "Prevalence and risk of severe cognitive impairment in advanced chronic kidney disease," The Journals of Gerontology: Series A, vol. 73, no. 3, pp. 393–399, 2018.
[6] A. van Zwieten, G. Wong, M. Ruospo, S. C. Palmer, M. R. Barulli, A. Iurillo, V. Saglimbene, P. Natale, L. Gargano, M. Murgo et al., "Prevalence and patterns of cognitive impairment in adult hemodialysis patients: the cognitive-hd study," Nephrology Dialysis Transplantation, vol. 33, no. 7, pp. 1197–1206, 2018.
[7] F. E. Tiffin Richards, A. S. Costa, B. Holschbach, R. D. Frank, A. Vassiliadou, T. Krüger, K. Kuckuck, T. Gross, F. Eitner, J. Floege et al., "The montreal cognitive assessment (moca)-a sensitive screening instrument for detecting cognitive impairment in chronic hemodialysis patients," PloS one, vol. 9, no. 10, p. e106700, 2014.
[8] Y. F. Shea, M. S. C. Lee, M. y. M. Mok, F. H. W. Chan, and T. M. Chan, "Prevalence of cognitive impairment among peritoneal dialysis patients: a systematic review and meta-analysis," Clinical and Experimental Nephrology, vol. 23, no. 10, pp. 1221–1234, 2019.
[9] M. L. Ries, C. M. Carlsson, H. A. Rowley, M. A. Sager, C. E. Gleason, S. Asthana, and S. C. Johnson, "Magnetic resonance imaging characterization of brain structure and function in mild cognitive impairment: a review," Journal of the American Geriatrics Society, vol. 56, no. 5, pp. 920–934, 2008.
[10] R. M. Hutchison, T. Womelsdorf, E. A. Allen, P. A. Bandettini, V. D. Calhoun, M. Corbetta, S. Della Penna, J. H. Duyn, G. H. Glover, J. Gonzalez Castillo et al., "Dynamic functional connectivity: promise, issues, and interpretations," Neuroimage, vol. 80, pp. 360–378, 2013.
[11] E. A. Allen, E. Damaraju, S. M. Plis, E. B. Erhardt, T. Eichele, and V. D. Calhoun, "Tracking whole-brain connectivity dynamics in the resting state," Cerebral cortex, vol. 24, no. 3, pp. 663–676, 2014.

[12] W. Li, Y. Chen, X. Xu, X. Wang, and X. Gao, "Human-guided functional connectivity network estimation for chronic tinnitus identification: a modularity view," IEEE Journal of Biomedical and Health Informatics, vol. 26, no. 10, pp. 4849–4858, 2022.
[13] W. Li, L. Qiao, L. Zhang, Z. Wang, and D. Shen, "Functional brain network estimation with time series self-scrubbing," IEEE journal of biomedical and health informatics, vol. 23, no. 6, pp. 2494–2504, 2019.
[14] W. Li, L. Zhang, L. Qiao, and D. Shen, "Toward a better estimation of functional brain network for mild cognitive impairment identification: a transfer learning view," IEEE journal of biomedical and health informatics, vol. 24, no. 4, pp. 1160–1168, 2019.
[15] W. Li, Z. Wang, L. Zhang, L. Qiao, and D. Shen, "Remodeling pearson's correlation for functional brain network estimation and autism spectrum disorder identification," Frontiers in neuroinformatics, vol. 11, p. 55, 2017.
[16] A. Elton and W. Gao, "Task-related modulation of functional connectivity variability and its behavioral correlations," Human brain mapping, vol. 36, no. 8, pp. 3260–3272, 2015.
[17] M. Díez-Cirarda, A. P. Strafella, J. Kim, J. Peña, N. Ojeda, A. Cabrera Zubizarreta, and N. Ibarretxe Bilbao, "Dynamic functional connectivity in parkinson's disease patients with mild cognitive impairment and normal cognition," NeuroImage: Clinical, vol. 17, pp. 847–855, 2018.
[18] Y. m. Wang, X. l. Cai, R. t. Zhang, Y. j. Zhang, H. y. Zhou, Y. Wang, Y. Wang, J. Huang, Y. y. Wang, E. F. Cheung et al., "Altered brain structural and functional connectivity in schizotypy," Psychological Medicine, vol. 52, no. 5, pp. 834–843, 2022.
[19] P. Mukli, C. B. Pinto, C. D. Owens, T. Csipo, A. Lipecz, Z. Szarvas, A. Peterfi, A. C. d. C. P. Langley, J. Hoffmeister, F. S. Racz et al., "Impaired neurovascular coupling and increased functional connectivity in the frontal cortex predict age-related cognitive dysfunction," Advanced Science, vol. 11, no. 10, p. 2303516, 2024.
[20] Y. Gu, Y. Lin, L. Huang, J. Ma, J. Zhang, Y. Xiao, Z. Dai, and A. D. N. Initiative, "Abnormal dynamic functional connectivity in alzheimer's disease," CNS neuroscience & therapeutics, vol. 26, no. 9, pp. 962–971, 2020.
[21] M. Kudela, J. Harezlak, and M. A. Lindquist, "Assessing uncertainty in dynamic functional connectivity," NeuroImage, vol. 149, pp. 165–177, 2017.
[22] V. M. Vergara, A. Abrol, and V. D. Calhoun, "An average sliding window correlation method for dynamic functional connectivity," Human Brain Mapping, vol. 40, no. 7, pp. 2089–2103, 2019.
[23] A. D. Savva, G. D. Mitsis, and G. K. Matsopoulos, "Assessment of dynamic functional connectivity in resting-state fmri using the sliding window technique," Brain and behavior, vol. 9, no. 4, p. e01255, 2019.
[24] J. Schumacher, J. P. Taylor, C. A. Hamilton, M. Firbank, P. C. Donaghy, G. Roberts, L. Allan, R. Durcan, N. Barnett, J. T. O'Brien et al., "Functional connectivity in mild cognitive impairment with lewy bodies," Journal of Neurology, vol. 268, no. 12, pp. 4707–4720, 2021.
[25] L. G. França, J. Ciarrusta, O. Gale Grant, S. Fenn Moltu, S. Fitzgibbon, A. Chew, S. Falconer, R. Dimitrova, L. Cordero Grande, A. N. Price et al., "Neonatal brain dynamic functional connectivity in term and preterm infants and its association with early childhood neurodevelopment," Nature Communications, vol. 15, no. 1, p. 16, 2024.
[26] S. Alonso Martínez, G. Deco, G. J. Ter Horst, and J. Cabral, "The dynamics of functional brain networks associated with depressive symptoms in a nonclinical sample," Frontiers in neural circuits, vol. 14, p. 570583, 2020.
[27] H. Yu, C. Zhang, Y. Cai, N. Wu, K. Duan, W. Bo, Y. Liu, and Z. Xu, "Abnormal regional homogeneity and amplitude of low frequency fluctuation in chronic kidney patients with and without dialysis," Frontiers in Neuroscience, vol. 16, p. 1064813, 2022.
[28] X. Zhang, L. Yang, J. Lu, Y. Yuan, D. Li, H. Zhang, R. Yao, J. Xiang, and B. Wang, "Reconfiguration of brain network dynamics in bipolar disorder: a hidden markov model approach," Translational Psychiatry, vol. 14, no. 1, p. 507, 2024.
[29] L. Qin, Q. Zhou, Y. Sun, X. Pang, Z. Chen, and J. Zheng, "Dynamic functional connectivity and gene expression correlates in temporal lobe epilepsy: insights from hidden markov models," Journal of Translational Medicine, vol. 22, no. 1, p. 763, 2024.
[30] G. Zhang, B. Cai, A. Zhang, J. M. Stephen, T. W. Wilson, V. D. Calhoun, and Y. P. Wang, "Estimating dynamic functional brain connectivity with a sparse hidden markov model," IEEE transactions on medical imaging, vol. 39, no. 2, pp. 488–498, 2019.
[31] S. F. Nielsen, M. N. Schmidt, K. H. Madsen, and M. Mørup, "Predictive assessment of models for dynamic functional connectivity," Neuroimage, vol. 171, pp. 116–134, 2018.
[32] M. Sourty, L. Thoraval, D. Roquet, J. P. Armspach, J. Foucher, and F. Blanc, "Identifying dynamic functional connectivity changes in dementia with lewy bodies based on product hidden markov models," Frontiers in computational neuroscience, vol. 10, p. 60, 2016.
[33] C. G. Yan, X. D. Wang, X. N. Zuo, and Y. F. Zang, "Dpabi: data processing & analysis for (resting-state) brain imaging," Neuroinformatics, vol. 14, no. 3, pp. 339–351, 2016.
[34] E. T. Rolls, C. C. Huang, C. P. Lin, J. Feng, and M. Joliot, "Automated anatomical labelling atlas 3," Neuroimage, vol. 206, p. 116189, 2020.
[35] Z. S. Nasreddine, N. A. Phillips, V. Bédirian, S. Charbonneau, V. Whitehead, I. Collin, J. L. Cummings, and H. Chertkow, "The montreal cognitive assessment, moca: a brief screening tool for mild cognitive impairment," Journal of the American Geriatrics Society, vol. 53, no. 4, pp. 695–699, 2005.
[36] D. Vidaurre, S. M. Smith, and M. W. Woolrich, "Brain network dynamics are hierarchically organized in time," Proceedings of the National Academy of Sciences, vol. 114, no. 48, pp. 12 827–12 832, 2017.
[37] M. Moretto, E. Silvestri, A. Zangrossi, M. Corbetta, and A. Bertoldo, "Unveiling whole-brain dynamics in normal aging through hidden markov models," Human Brain Mapping, vol. 43, no. 3, pp. 1129–1144, 2022.
[38] B. T. Yeo, F. M. Krienen, J. Sepulcre, M. R. Sabuncu, D. Lashkari, M. Hollinshead, J. L. Roffman, J. W. Smoller, L. Zöllei, J. R. Polimeni et al., "The organization of the human cerebral cortex estimated by intrinsic functional connectivity," Journal of neurophysiology, 2011.

DANJIE SUN received the B.S. degree in Information and Computational Science from Chongqing Jiaotong University in 2024. She is currently pursuing the M.S. degree in Systems Science at Chongqing Jiaotong University. Her research interests include brain network construction and analysis.

WEIKAI LI received his B.S. degree in Information and Computing Science from Chongqing Jiaotong University in 2015. In 2018, he completed his M.S. degree in computer science and technique at Chongqing Jiaotong University. In 2022, he completed his Ph.D. degree with the College of Computer Science & Technology, Nanjing University of Aeronautics and Astronautics. He is now a lecturer at the School of Mathematics and Statistics, Chongqing Jiaotong University. His research interests include pattern recognition and machine learning.

HUAN YU is an Associate Chief Physician in Imaging and Nuclear Medicine. She received the B.S. degree in Medical Imaging from Harbin Medical University in 2009, the M.S. degree in Imaging and Nuclear Medicine from the Second Military Medical University in 2012, and the Ph.D. degree in Imaging and Nuclear Medicine from Capital Medical University in 2023. She is currently a Postdoctoral Research Fellow at Zhongda Hospital, Southeast University, and also serves at Liangxiang Teaching Hospital, Capital Medical University. Her research interests include neuroimaging and abdominal imaging.

XIAOFENG CHEN was born in 1980. He received the B.S. degree in Mathematics in 2003 and the M.S. degree in Applied Mathematics in 2006 both from Sichuan University, Chengdu, China. From July 2006 to now he is with Department of Mathematics, Chongqing Jiaotong University, Chongqing, China. His current research interest involves stability theory of complex-valued and quaternion-valued neural networks.

CHAOYANG ZHANG is a Chief Physician in Nephrology. He received the B.S. degree in Clinical Medicine from Chengde Medical University in 2006, the M.S. degree in Internal Medicine from the Second Military Medical University in 2013, and the Ph.D. degree in Nephrology from the Chinese PLA Medical School in 2024. He is currently with BOE Hospital. His research interests include the intersection of nephrology and neurological disorders, as well as clinical diagnosis and treatment strategies.